

Cite this: *Dalton Trans.*, 2025, **54**, 889

# Emerging frontiers of nickel–aluminium layered double hydroxide heterojunctions for photocatalysis

Chunxue Li,<sup>a</sup> Guixiang Ding,<sup>b</sup> Peng Wang,<sup>c</sup> Kun Liu,<sup>\*d</sup> Bin Yang<sup>\*e</sup> and Guangfu Liao<sup>\*b</sup>

The unique benefits of nickel–aluminium layered double hydroxide (Ni–Al LDH)-based heterojunctions, including large surface area, tunable bandgap and morphology, abundant reaction sites, and high activity, selectivity, and photostability, make them extremely promising for photocatalytic applications. Given the importance and benefits of Ni–Al LDH-based heterojunctions in photocatalysis, it is necessary to provide a summary of Ni–Al LDH-based heterojunctions for photocatalytic applications. Hence, in this review, we thoroughly described the material design for Ni–Al LDH-based heterojunctions, along with their recent developments in various photocatalytic applications, *i.e.*, H<sub>2</sub> evolution, CO<sub>2</sub> reduction, and pollutant removal. Moreover, the most recent advancements, difficulties, and future prospects of Ni–Al LDH-based heterojunctions for photocatalytic applications were emphasized and thoroughly examined. Undoubtedly, in the near future, scientific researchers will put relentless efforts to exploit new Ni–Al LDH-based heterojunctions for high-performance photocatalytic applications.

Received 10th November 2024,  
Accepted 19th December 2024

DOI: 10.1039/d4dt03141e

rsc.li/dalton

## 1. Introduction

Layered double hydroxides (LDHs), a unique class of nanomaterials, are made up of positively charged layers with charge-balancing anions in the interlayer voids and have been widely used for photocatalysis owing to their large surface area, tunable bandgap and morphology, abundant reaction sites, good stability, *etc.*<sup>1,2</sup> Compared to other LDHs, nickel–aluminum layered double hydroxides (Ni–Al LDHs) are one of the most reported LDH-based photocatalysts because they show a more stable structure and can maintain their structure and photoactivity for a long time. Moreover, the physicochemical characteristics and photocatalytic performances of Ni–Al LDHs are easier to optimize by precisely controlling the Ni/Al ratio during synthesis.<sup>3</sup> Furthermore, the Ni–Al LDHs are a typical n-type semiconductor, which shows a narrow band

structure for a wide range of light absorption.<sup>4,5</sup> In addition, the Ni site in the Ni–Al LDHs shows stronger adsorption effects for CO<sub>2</sub>, thus exhibiting huge application prospects in CO<sub>2</sub> photoreduction.<sup>6</sup> However, many challenges, for instance, weak conductivity, fast photogenerated carrier recombination and low light responsiveness, hamper their photocatalytic performances. Thus, exploring suitable methods to solve these problems is crucial.

More promising techniques, such as loading noble metal nanoparticles, introducing defects, doping elements, and creating heterojunctions, were developed as a result of the recent researches on photocatalysts.<sup>2,7</sup> Because of their advantages in improving light absorption, decreasing photogenerated carrier recombination, and encouraging photogenerated carrier separation, Ni–Al LDH-based heterojunctions are considered a promising approach among them.<sup>8</sup> For example, Li and co-workers reported the construction of a carbon dot (CD)/Ni–Al LDH@In<sub>2</sub>O<sub>3</sub> S-scheme heterojunction in a multi-shell nanotube heterostructure, which showed the CH<sub>4</sub> and CO production rates of 10.67 μmol g<sup>-1</sup> h<sup>-1</sup> and 7.12 μmol g<sup>-1</sup> h<sup>-1</sup>, respectively, which were 1.15 fold greater than those of a single Ni–Al LDH.<sup>9</sup> Therefore, the unique structure and fascinating photocatalytic mechanism of Ni–Al LDH-based heterojunctions have garnered significant attention and found various photocatalytic applications, such as H<sub>2</sub> evolution, CO<sub>2</sub> reduction, and pollutant removal.

Our work outlines the progress made in Ni–Al LDH-based heterojunctions for photocatalysis in recent years in. Firstly,

<sup>a</sup>College of Ecological Environment and Urban Construction, Fujian University of Technology, Fuzhou 350118, China

<sup>b</sup>National Forestry and Grassland Administration Key Laboratory of Plant Fiber Functional Materials, College of Materials Engineering, Fujian Agriculture and Forestry University, Fuzhou 350002, China. E-mail: liaogf@mail2.sysu.edu.cn

<sup>c</sup>Shandong Chambroad Petrochemicals Co., Ltd, Binzhou, Shandong 256500, China

<sup>d</sup>School of Resources and Environment, Nanchang University, 999 Xuefu Road, Nanchang, Jiangxi, 330031, China. E-mail: liukun@ncu.edu.cn

<sup>e</sup>School of Chemistry and Chemical Engineering/State Key Laboratory Incubation Base for Green Processing of Chemical Engineering, Shihezi University, Shihezi 832003, China. E-mail: yangbin@shzu.edu.cn

the material design including the fundamental principle, band alignment, and synthetic strategies for Ni–Al LDH-based heterojunctions is presented. Then, the achievements in recent years in terms of photocatalytic applications, such as H<sub>2</sub> evolution, CO<sub>2</sub> reduction, and pollutant removal are briefly discussed. Finally, we provide constructive comments and discuss the future development and challenges in the field.

## 2. Material design for Ni–Al LDH-based heterojunctions

### 2.1. The fundamental principle of photocatalysis

Photocatalysis involves four main processes:<sup>10–13</sup> light collection, charge separation, charge migration, and use of charge for redox processes. When a semiconductor is exposed to photons with energy ( $h\nu$ ) equal to or greater than its band gap ( $E_g$ ) energy, photogenerated electron ( $e^-$ )-hole ( $h^+$ ) pairs are created, with  $e^-$  in the conduction band (CB) and  $h^+$  in the valence band (VB). The delocalization of these  $e^-$ - $h^+$  couples allows them to separate into independent charges. Some of them can migrate to the surface of the photocatalyst, where they interact chemically with the adsorbed species in a variety of ways, resulting in reduction and oxidation processes. Accelerating the separation and migration of photogenerated charges and lowering their recombination rate are essential for greatly increasing the photocatalytic efficiency. Additionally, increasing light absorption can greatly boost the photocatalytic efficiency.

A semiconductor having a more positive VB potential and a more negative CB potential is said to have a wider band-gap.<sup>14,15</sup> Since solar energy conversion efficiency makes up 43% of the total solar energy, this results in an apparent decrease in the amount of solar radiation used in the visible spectrum. For instance, anatase TiO<sub>2</sub> exclusively uses sunlight in the ultraviolet (UV) region, which makes up less than 5% of the solar spectrum, and has a broad  $E_g$  of 3.2 eV.<sup>16</sup> Therefore, it is challenging to simultaneously enhance the photocatalytic properties of a single-component photocatalyst due to the apparent contradiction between redox capabilities and light absorption. Another intrinsic property that significantly affects the photocatalytic effectiveness of the single-component photocatalyst is quick charge recombination. Approximately 90% of the  $e^-$  and  $h^+$  quickly recombine at the surface when charges are migrated and transferred there. It is insufficient to drive the chemical reactions because the photocatalyst surface can only receive less than 10% of the separated charges. Constructing suitable heterogeneous photocatalytic systems has been shown to be an effective way to tackle these issues because they not only inhibit the recombination of photocarriers but provide the photocatalysts with certain unique characteristics.<sup>3</sup> Because of their reasonable design, Ni–Al LDH-based heterojunctions can therefore present interesting paths for the development of efficient photocatalysts.

### 2.2. Band alignment and type of Ni–Al LDH-based heterojunctions

As shown in Fig. 1a–c, the Ni–Al LDH-based heterojunction formed between two semiconductors is classified into three types based on the band alignment between their CBs and VBs: straddling-gap heterojunction (type I), staggered-gap heterojunction (type II), and broken-gap heterojunction (type III).<sup>17</sup> In these three heterojunctions, the semiconductor's smaller band-gap leads  $e^-$  and  $h^+$  to accumulate, increasing the possibility of recombination and, eventually, diminishing the photocatalytic efficiency. In type II heterojunctions,  $e^-$  and  $h^+$  are transferred to their respective low energy bands; Ni–Al LDH with an appropriate  $E_g$  of around 2.7 eV concentrates  $e^-$ , whereas photosystem A (PS A) accumulates  $h^+$ . The physical separation of the photocarriers will increase the photocatalytic efficiency, but the redox performance will be reduced when  $e^-$  and  $h^+$  congregate in bands with low energy potentials. Since there is no charge migration between the  $e^-$  and  $h^+$  in a type III heterojunction, the two constituent semiconductors operate separately. Furthermore, a Z-scheme heterojunction is formed when two semiconductors with interlaced band alignment come into close contact and charge transfer occurs between the VB in PS A and the CB in Ni–Al LDH (Fig. 1d). Unlike type II heterojunctions, Z-scheme heterojunctions allow photogenerated  $e^-$  in Ni–Al LDH to migrate before mixing with photogenerated  $h^+$  in PS A.<sup>18,19</sup>

### 2.3. Synthetic strategy of Ni–Al LDH-based heterojunctions

Choosing a suitable synthesis approach is essential to optimize the NiAl LDH-based heterojunction and enhance its photocatalytic performance. The photocatalytic performance of NiAl LDH-based heterojunctions prepared through these technologies is greatly impacted by the modifications required to regulate the chemical composition, surface area, crystallinity, and morphology. Researching these synthesis methods can lead to the development of a unique NiAl LDH-based heterojunction with increased photocatalytic efficiency and a wider range of applications.

**2.3.1. Hydrothermal method.** The Ni–Al LDH prepared through the hydrothermal method can be further modified to form Ni–Al LDH-based heterojunctions with various morphologies. For example, Liu and co-workers<sup>20</sup> successfully fabricated a Ni–Al LDH/Ag<sub>6</sub>Si<sub>2</sub>O<sub>7</sub> S-scheme heterojunction through a simple hydrothermal strategy (Fig. 2a). This strategy helps to suppress the aggregation effects of Ag<sub>6</sub>Si<sub>2</sub>O<sub>7</sub> through uniform distribution on the surface of the Ni–Al LDH microsphere, thus showing excellent photocatalytic performance. Moreover, a ZnO/ZnS/Ni–Al LDH ternary heterojunction was also fabricated in core-shell morphology using adjusted hydrothermal approaches.<sup>21</sup> In this case, the positively charged lamellar Ni–Al LDH was uniformly loaded on negatively charged ZnO/ZnS rods. The ternary core-shell rod-like structure promoted the formation of a heterojunction at interfaces through exposing more catalytically active sites and establish-

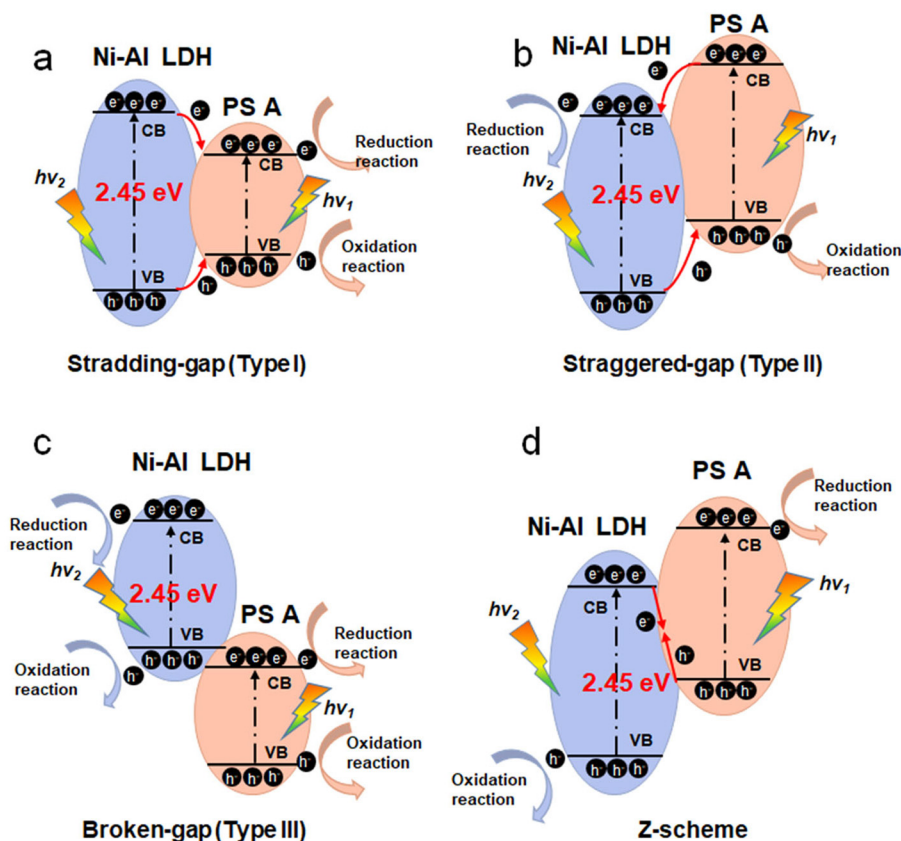


Fig. 1 Band configurations and charge flow directions in Ni–Al LDH-based (a) type I, (b) type II, (c) type III, and (d) Z-scheme heterojunctions.

ing extremely tight contact, which improved the photocatalytic activity.

**2.3.2. Solvothermal method.** The solvothermal method is also an effective strategy for the construction of Ni–Al LDH-based heterojunctions with a controllable morphology. In comparison to the hydrothermal method, the solvothermal method uses organic solvents with higher temperature to fabricate Ni–Al LDH-based heterojunctions, which shows greater applicability. Recently, Li and co-workers<sup>22</sup> proposed an atomic activation solvothermal approach to develop a flower-like Ni–Al LDH/CeO<sub>2</sub> heterojunction for selective CH<sub>4</sub> photosynthesis. It was of great importance that the decorated CeO<sub>2</sub> nanoparticles could optimize the electronic structure and activate the originally inert Ni and Al atoms on Ni–Al LDH, acting as the potential active centers. This work provides an atomic activation strategy to develop LDH-based heterojunctions, which reveals a new insight to develop efficient heterojunction systems for CO<sub>2</sub> photoreduction.

**2.3.3. Co-precipitation method.** A common technique for creating Ni–Al LDH-based heterojunctions in sheet-like structures is the co-precipitation method. Upon adding base materials (such as NaOH) to alkaline solutions with pH values typically between 9 and 11, the co-precipitation approach combines the Ni and Al precursors to form gel-like precipitates

under vigorous stirring.<sup>3</sup> The co-precipitation strategy has recently been used to construct a LaOCl/Ni–Al LDH heterojunction with a cladding structure by immobilizing Ni–Al LDH nanosheets on LaOCl flakes.<sup>23</sup> The photocatalytic reaction and stability of composite materials are enhanced by this heterostructure, which offers regional pathways for charge transfer between Ni–Al LDH and LaOCl *via* their close interface. Moreover, a chloride intercalated Ni–Al LDH with a good laminated structure and excellent water dispersibility was successfully constructed through a simple co-precipitation strategy (Fig. 2b).<sup>24</sup> This work proposed an effective method for the remediation of water polluted with antimony using Ni–Al LDH-based materials.

**2.3.4. Calcination method.** The calcination strategy is the process of heating materials under specified process circumstances and procedures to change their physical and chemical properties,<sup>25,26</sup> which is commonly used in the fabrication of Ni–Al LDH-based heterojunctions. Recently, a novel dual S-scheme heterojunction photocatalyst  $\alpha$ -Bi<sub>2</sub>O<sub>3</sub>/NiAl-LDH consisting of phase-transformed bismuth oxide combined with layered double hydroxides has been successfully fabricated through the solvothermal-calcination method (Fig. 2c).<sup>27</sup> The creation of an S-scheme heterostructure results in the formation of internal electric fields (IEFs) between the interfaces as well as the bending of the band edges, which is highly

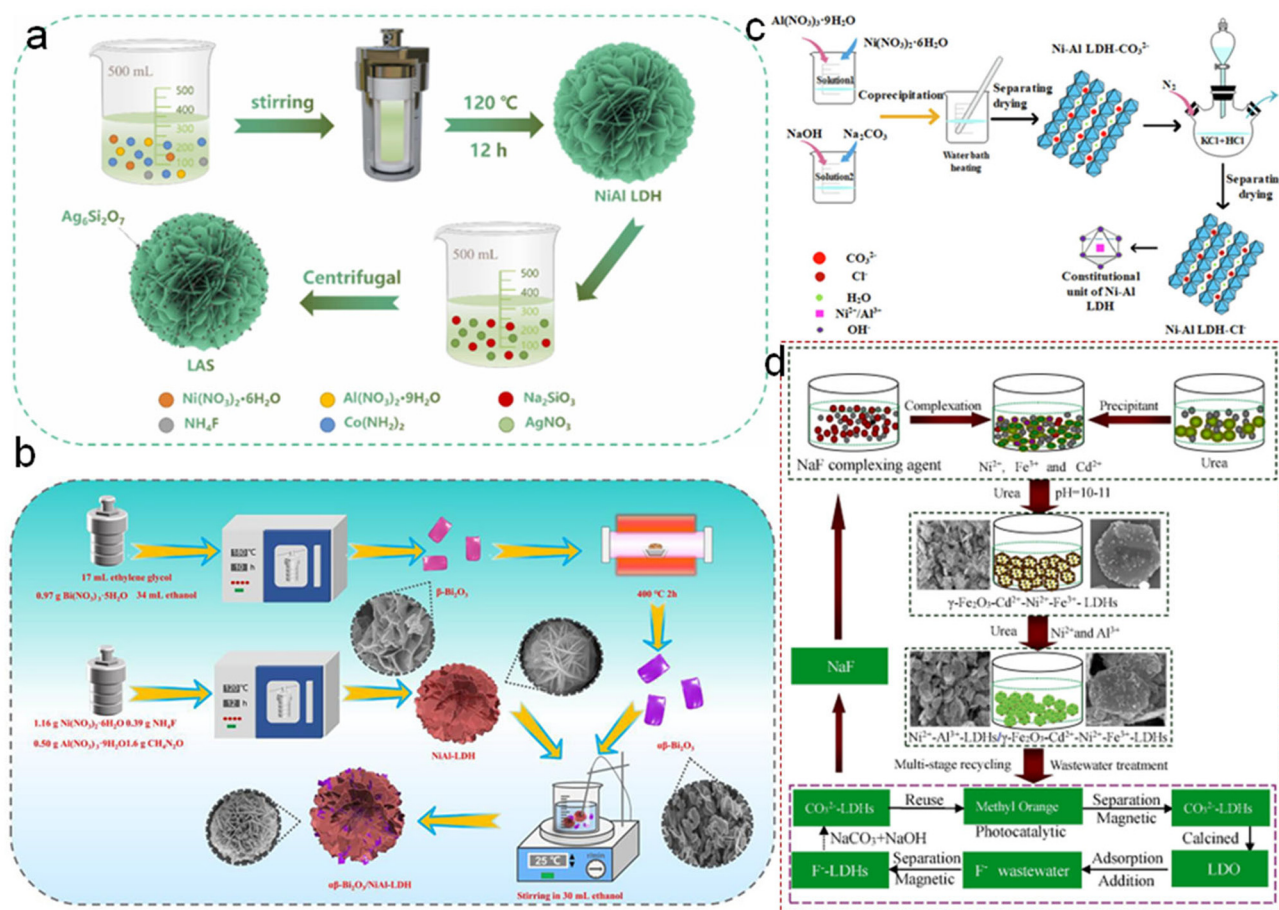


**Fig. 2** (a) Hydrothermal method for the construction of the Ni–Al LDH-based heterojunction. Reproduced with permission from ref. 20. (b) Co-precipitation method for the construction of Ni–Al LDH-based heterojunctions. Reproduced with permission from ref. 24. (c) Calcination method for the construction of Ni–Al LDH-based heterojunctions. Reproduced with permission from ref. 27. (d) Ion exchange method for the construction of Ni–Al LDH-based heterojunctions. Reproduced with permission from ref. 30.

advantageous for the separation and extension of photogenerated carriers.

**2.3.5. Ion exchange method.** Ion exchange is primarily concerned with changing out the ions within an ionic crystal, but it also preserves the framework between them.<sup>28,29</sup> Thus, the ion exchange strategy has been widely used for the fabrication of the Ni–Al LDH-based heterojunction. An innovative, simple, and economic ion exchange approach was reported for producing highly crystalline magnetic  $\gamma$ -Fe<sub>2</sub>O<sub>3</sub>-Cd<sup>2+</sup>-Ni<sup>2+</sup>-Fe<sup>3+</sup> LDH from cation chloride salts and F<sup>-</sup> added as a complexing agent (Fig. 2d).<sup>30</sup> The prepared Ni<sup>2+</sup>-Al<sup>3+</sup> LDH/ $\gamma$ -Fe<sub>2</sub>O<sub>3</sub>-Cd<sup>2+</sup>-Ni<sup>2+</sup>-Fe<sup>3+</sup> LDH is a promising adsorbent for methyl orange degradation and F<sup>-</sup> removal in practical remediation of wastewaters due to its simple synthesis, nontoxicity, low cost, recyclability, and high removal capability.

**2.3.6. Electrospinning method.** We are aware that electrospinning is a simple and effective method for producing one-dimensional (1D) materials such as nanotubes, nanofibers, and nanobelts.<sup>31,32</sup> It can also be utilized to make Ni–Al LDH-based heterojunctions. To achieve the synergistic effect of compositions and microstructures, hybrid materials made of Ni

embedded carbon nanofibers/Ni–Al LDH were successfully prepared by the electrospinning method.<sup>33</sup> This work offers a novel perspective for improving the electrical conductivity of electrodes and constructing Ni–Al LDH-based heterojunctions.

Among various fabrication approaches, hydrothermal and solvothermal, co-precipitation, calcination, and ion-exchange methods benefit from a close and robust contact between Ni–Al LDH and other semiconductors, improving their photocarrier migration efficiency. Different strategies can produce Ni–Al LDH-based heterojunctions with different chemical compositions, surface areas, crystallinities, and morphologies for achieving unique optoelectronic and physicochemical properties, which is beneficial for further photocatalytic applications. For example, the electrospinning technique can create a 1D Ni–Al LDH-based heterojunction, allowing for the faster migration of photogenerated charges in one direction. Strong interactions, *i.e.*, covalent bonds, ionic bonds, and coordination bonds, and weak interactions, *i.e.*, hydrogen bonds and van der Waals forces, can be formed between Ni–Al LDH and other semiconductors, which serve as charge transfer pathways and enhance interface contact.

### 3. Ni–Al LDH-based heterojunctions for photocatalytic applications

According to an earlier example, the creation of a Ni–Al LDH-based heterojunction can maintain its high redox ability and visible light absorption while also speeding up the separation of photogenerated carriers. Consequently, the Ni–Al LDH-based heterojunction shows great promise for photocatalysis. The limitless solar energy is the primary catalyst needed for photocatalytic processes. The numerous photocatalytic uses of the Ni–Al LDH-based heterojunction are outlined and thoroughly examined in the following subsections.

#### 3.1. Photocatalytic water splitting

Given the depletion of traditional fossil fuels and the increasing demand for clean and sustainable H<sub>2</sub> energy sources, Ni–Al LDH-based heterojunctions have become increasingly impor-

tant in the field of photocatalytic water splitting.<sup>34,35</sup> In the following section, we will briefly introduce some classic Ni–Al LDH-based heterojunctions for photocatalytic water splitting.

The Ni–Al LDH-based materials have attracted more attention in photocatalysis due to their low cost, wide band gaps, and adjustable photocatalytic active sites; however, their low photogenerated carrier separation efficiency limits their photocatalytic efficiency. Recently, our group has reported a Ni–Al LDH/Ni-doped Zn<sub>0.5</sub>Cd<sub>0.5</sub>S (LDH/Ni-ZCS) S-scheme heterojunction for effective photocatalytic H<sub>2</sub> evolution (Fig. 3a).<sup>36</sup> The 15% LDH/1% Ni-ZCS displays comparable photocatalytic hydrogen evolution activity with a rate of 6584 μmol g<sup>-1</sup> h<sup>-1</sup>, which outperforms most of the previously reported LDH-based and metal sulfide-based photocatalysts (Fig. 3c–h). The manufacturing of the S-scheme heterojunction not only speeded up the separation of photogenerated carriers, but it also reduced the activation energy of H<sub>2</sub> production and increased redox capacity (Fig. 3b). Moreover, a binary CoS<sub>x</sub>/NiAl-LDH S-scheme

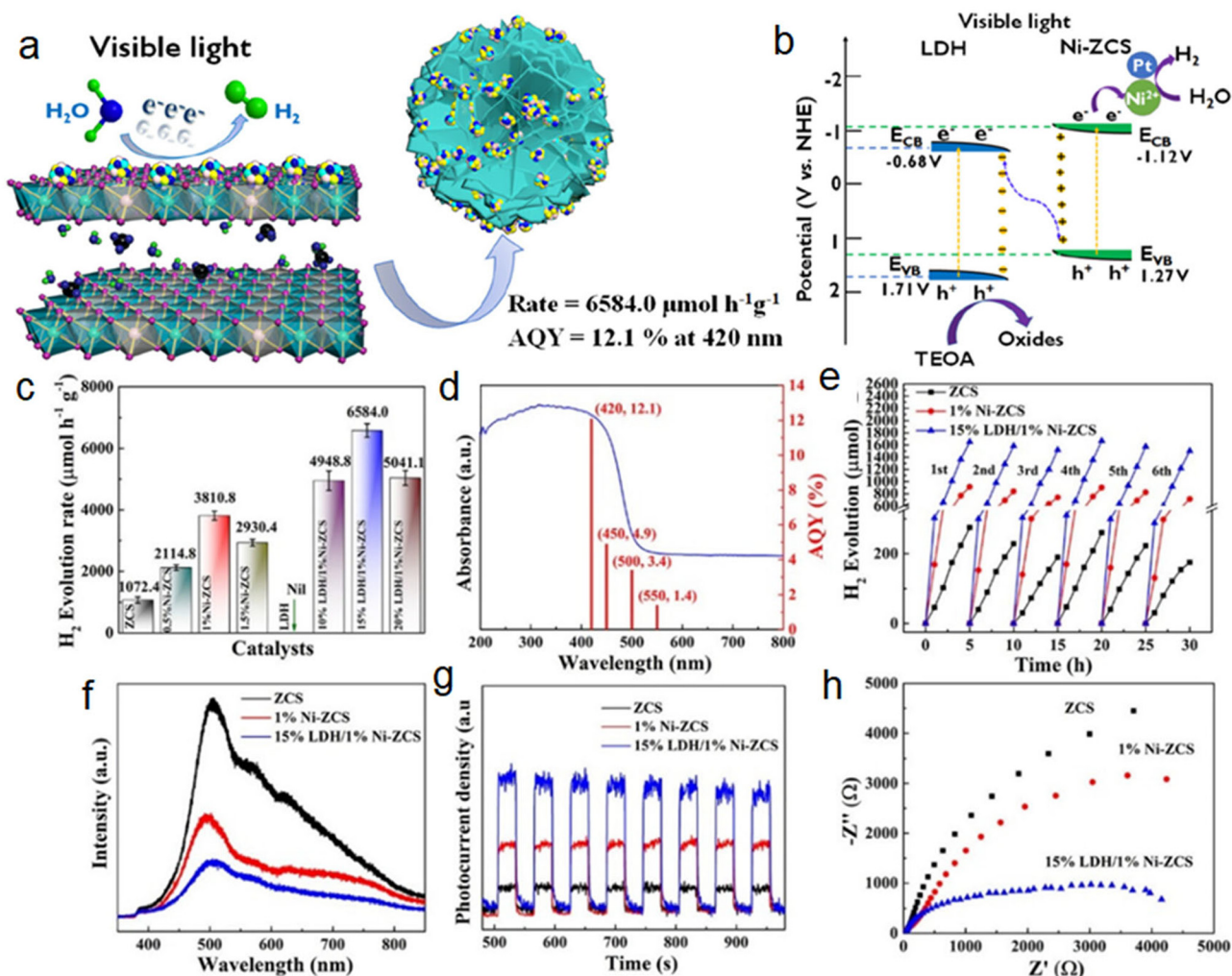


**Fig. 3** (a) Ni–Al LDH/Ni-doped Zn<sub>0.5</sub>Cd<sub>0.5</sub>S S-scheme heterojunction for effective photocatalytic H<sub>2</sub> evolution. (b) Proposed photocatalytic mechanism for the enhancement of photocatalytic performance. (c) Photocatalytic production rates of different samples. (d) Quantum yield (AQY) of 15% LDH/1% Ni-ZCS. (e) Stability test over ZCS, 1% Ni-ZCS, and 15% LDH/1% Ni-ZCS. (f) Photoluminescence (PL) spectra, (g) photocurrent curves, and (h) electrochemical impedance spectroscopy (EIS) curves of ZCS, 1% Ni-ZCS, and 15% LDH/1% Ni-ZCS. Reproduced with permission from ref. 36.

heterojunction also reached  $3678.59 \mu\text{mol g}^{-1} \text{h}^{-1}$ , which was 83.74 and 22 times the rates of  $\text{CoS}_x$  and NiAl-LDH, respectively.<sup>37</sup>

Although the photocatalytic  $\text{H}_2$  production by the Ni–Al LDH-based heterojunction has been widely reported, its complementary reaction photocatalytic  $\text{O}_2$  evolution is more difficult to achieve due to the multiple reaction steps of four holes.<sup>38,39</sup> Recently, Ramesh and co-workers<sup>40</sup> have designed a NiAl-LDH/g-C<sub>3</sub>N<sub>4</sub>/Ag<sub>3</sub>PO<sub>4</sub> dual direct Z-scheme heterojunction, which serves as the  $\text{H}_2$  and  $\text{O}_2$  evolution photocatalyst. The prepared dual direct Z-scheme heterojunction displayed improved photocatalytic performance for overall water splitting. This work not only reported overall water splitting using the Ni–Al LDH-based heterojunction but it also provided experimental evidence for understanding the possible reaction process and the mechanism of photocatalytic water splitting.

### 3.2. Photocatalytic CO<sub>2</sub> reduction

Inspired by natural photosynthesis, photocatalytic CO<sub>2</sub> reduction to useful carbon sources by Ni–Al LDH-based heterojunctions is a very promising strategy for alleviating the greenhouse effect due to their high surface area, tunable composition, and exposed active sites.<sup>29,41,42</sup> For example, a novel NiAl-LDH/Ti<sub>3</sub>C<sub>2</sub>T<sub>x</sub> nanosheet (NiAl-LDH/TNS) with a core–shell structure was successfully prepared through an *in situ* hydrothermal strategy (Fig. 4a).<sup>43</sup> In this case, NiAl-LDH coupled with Ti<sub>3</sub>C<sub>2</sub>T<sub>x</sub> nanosheets to form a Schottky junction could suppress the back-diffusion of electrons and facilitate the transfer of charge carriers (Fig. 4b). Benefiting from this feature, the optimized sample with the Ti<sub>3</sub>C<sub>2</sub>T<sub>x</sub> additive

amount of 75 mg possessed a photocatalytic CO<sub>2</sub>-to-CO conversion rate of  $2128.46 \mu\text{mol h}^{-1} \text{g}^{-1}$  with a selectivity of 90.2% (Fig. 4c–f). Moreover, a defective Cu<sub>2–x</sub>S/Ni–Al-LDH heterojunction was also reported to exhibit outstanding CO<sub>2</sub> photoreduction performance in both the full-spectrum and near-infrared (NIR) regions.<sup>44</sup> Besides, a unique multiflower-like ReS<sub>2</sub>/NiAl-LDH heterojunction was intricately designed and synthesized *via* hydrothermal methods for improved photocatalytic CO<sub>2</sub> reduction.<sup>45</sup> The findings of this study provide useful insights and pave the way for future research into the design and construction of LDH-based heterojunctions for efficient CO<sub>2</sub> photoreduction.

Exploration of prospective photocatalysts with high efficiency and selectivity for CO<sub>2</sub> photoreduction is critical for tackling the energy crisis and other environmental issues caused by traditional fossil fuels.<sup>2,46,47</sup> Tonda and co-workers<sup>48</sup> reported a core–shell heterojunction where anatase TiO<sub>2</sub> hollow spheres served as the core component and Ni–Al LDH nanoflakes served as the shell component. The prepared TiO<sub>2</sub>/Ni–Al LDH core–shell heterojunction displayed a strong light-harvesting ability, large surface area, porous structure, and extraordinary CO<sub>2</sub> adsorption capability, which provided a broader platform for efficient charge transfer. Benefiting from these structural and compositional features, the TiO<sub>2</sub>/Ni–Al LDH core–shell heterojunction showed remarkable CO<sub>2</sub> reduction activity, high selectivity and stability. This work offers a promising approach to the rational design and fabrication of Ni–Al LDH core–shell heterojunctions with potential applications in solar energy conversion and environmental protection.

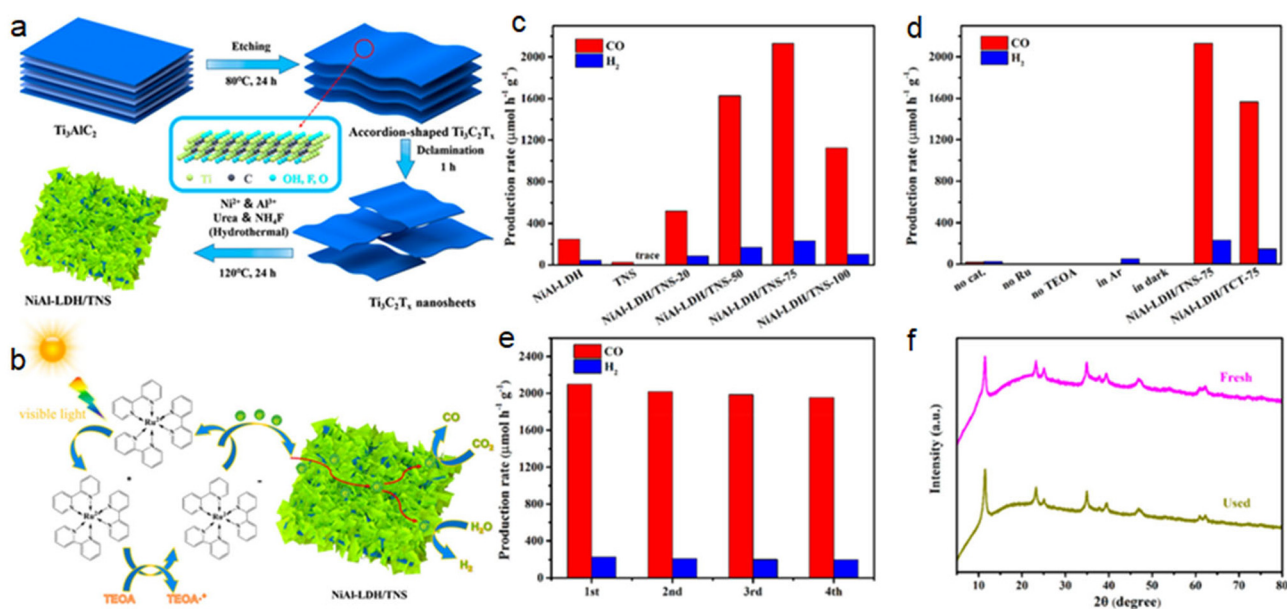


**Fig. 4** (a) Schematic of the synthetic process of NiAl-LDH/TNS. (b) Proposed mechanism of NiAl-LDH/TNS with [Ru(bpy)<sub>3</sub>]Cl<sub>2</sub> for CO<sub>2</sub> photoreduction. (c) Photoreduction performance of NiAl-LDH/TNS with different TNS content in the samples. (d) Production rates of CO and H<sub>2</sub> under various reaction conditions. (e) Production rates of CO and H<sub>2</sub> in stability tests. (f) XRD patterns of NiAl-LDH/TNS-75 before and after the CO<sub>2</sub> photoreduction experiment. Reproduced with permission from ref. 43.

Table 1 Comparison of the photocatalytic performance of Ni–Al LDH-based heterojunctions

Photocatalysts	Preparation method	Cocatalysts	Mass (mg)	Light source	Aqueous reaction	Photocatalytic activity	Apparent quantum yield (%)	Ref.
LDH/Ni-ZCS	Hydrothermal method	1 wt% Pt	50	300 W Xe lamp (>420 nm)	20 vol% TEOA	H <sub>2</sub> , 6584 μmol g <sup>-1</sup> h <sup>-1</sup>	12.1% (420 nm)	36
NiAl-LDH/CoS <sub>x</sub>	Solvothermal method	—	15	5 W white light (>420 nm)	TEOA and EY	H <sub>2</sub> , 3678.59 μmol g <sup>-1</sup> h <sup>-1</sup>	—	37
NiAl-LDH/g-C <sub>3</sub> N <sub>4</sub> /Ag <sub>2</sub> PO <sub>4</sub>	Calcination method	—	50	250 W quartz tungsten halogen lamp	10 vol% CH <sub>3</sub> OH (hole scavenger) and 0.05 M AgNO <sub>3</sub> (electron scavenger)	H <sub>2</sub> , 268 μmol g <sup>-1</sup> h <sup>-1</sup> and O <sub>2</sub> , 4330 μmol g <sup>-1</sup> h <sup>-1</sup>	1.29% (H <sub>2</sub> ) and 41.71% (O <sub>2</sub> )	40
NiAl-LDH/TNS	Hydrothermal method	—	7.5	300 W Xe lamp (>420 nm)	16.7 vol% TEOA	CO, 2128.46 μmol g <sup>-1</sup> h <sup>-1</sup> and H <sub>2</sub> , 230.68 μmol g <sup>-1</sup> h <sup>-1</sup>	—	43
Cu <sub>2-x</sub> S/Ni-Al-LDH	Hydrothermal method	—	50	300 W Xe lamp (>420 nm)	—	CO, 14.2 μmol g <sup>-1</sup> h <sup>-1</sup> and CH <sub>4</sub> , 5.3 μmol g <sup>-1</sup> h <sup>-1</sup>	3.86% (420 nm)	44
ReS <sub>2</sub> /NiAl-LDH	Hydrothermal method	—	10	300 W Xe lamp (>420 nm)	20 vol% TEOA	CO, 272.26 μmol g <sup>-1</sup> h <sup>-1</sup>	1.47% (420 nm)	45
TiO <sub>2</sub> /Ni-Al LDH	Hydrothermal and calcination method	—	50	300 W Xe lamp (>420 nm)	—	CO, 2.48 μmol g <sup>-1</sup> h <sup>-1</sup> and CH <sub>4</sub> , 20.56 μmol g <sup>-1</sup> h <sup>-1</sup>	—	48
g-C <sub>3</sub> N <sub>4</sub> @Ni-Al LDH	Co-precipitation method	—	600	500 W high-pressure Hg lamp	—	K <sub>app</sub> : 0.0192 min <sup>-1</sup> for Rh B and 0.0256 min <sup>-1</sup> for MO	—	50
NiAl-LDH/(BiO) <sub>2</sub> CO <sub>3</sub>	Hydrothermal method	—	50	500 W Xe lamp	—	K <sub>app</sub> : 0.01193 min <sup>-1</sup> for TC	—	51
BiOCl/NiAl-LDH	Mechanical mixing method	—	500	—	—	K <sub>app</sub> : 0.0089 min <sup>-1</sup> for MO, 0.008 min <sup>-1</sup> for MB, and 0.1874 min <sup>-1</sup> for LVX	—	53

TEOA: triethanolamine; EY: eosin Y; K<sub>app</sub>: reaction rate constant.

### 3.3. Photocatalytic pollutant removal

Many pollutants, including methylene blue (MB), methyl orange (MO), 4-nitrophenol (4-NP), tetracycline (TC), and rhodamine B (RhB), have recently been excessively discharged into soil and water, which has serious consequences for the environment and human health.<sup>26,49</sup> Ni–Al LDH-based heterojunctions have gained growing attention for pollutant removal due to their improved photocatalytic efficiency and stability. To design a promising Ni–Al LDH-based photocatalyst, Mahjoub and co-workers<sup>50</sup> synthesized a g-C<sub>3</sub>N<sub>4</sub>@Ni–Al LDH heterojunction with various g-C<sub>3</sub>N<sub>4</sub> contents. The synthesized photocatalyst showed excellent photocatalytic activity and stability for Rh B and MO degradation. Moreover, the NiAl-LDH nanosheets were uniformly grown on the (BiO)<sub>2</sub>CO<sub>3</sub> matrix, successfully forming a series of NiAl-LDH/(BiO)<sub>2</sub>CO<sub>3</sub> Z-scheme heterojunctions. When the mass fraction of (BiO)<sub>2</sub>CO<sub>3</sub> reached 25%, the prepared heterojunction showed superior performance (0.01193 min<sup>-1</sup>) and excellent stability for TC photodegradation.<sup>51</sup> More radicals and active sites for photocatalytic reactions can be produced by the Z-scheme heterojunction, which can also efficiently increase the separation efficiency of photogenerated charge-hole pairs and produce more active electrons and holes. Antibiotics are anticipated to be eliminated from real water bodies using this technique.

It has been demonstrated that a workable method for increasing the photocatalytic activity is the two-dimensional (2D)/2D van der Waals heterojunction.<sup>52</sup> Recently, a 2D/2D van der Waals BiOCl/NiAl-LDH S-scheme heterojunction with a sheet-on-sheet interface contact has been prepared by the mechanical mixing method.<sup>53</sup> Compared to pure BiOCl and NiAl-LDH, the BiOCl/NiAl-LDH S-scheme heterojunction exhibited improved photocatalytic activities for the degradation of an anionic dye (*i.e.*, MO), a cationic dye (*i.e.*, MB) and an antibiotic (*i.e.*, levofloxacin (LVX)). The enhancement in photocatalytic activity was attributed to the well-matched band structure and large contact area between BiOCl and NiAl-LDH. This work proved that the mechanical mixing method can simplify the preparation process of 2D/2D van der Waals heterojunctions, which provides a feasible way for future design and synthesis of high-efficiency Ni–Al LDH-based photocatalysts.

Combining the above results, the Ni–Al LDH-based heterojunction is a very promising photocatalyst for various applications due to its acceptable catalytic properties, favorable morphology in nanosheets and hierarchical microspheres, and thermal and chemical stability (Table 1).<sup>3</sup> Moreover, the photocatalytic performance of Ni–Al LDH can be simply optimized *via* precisely controlling the Ni/Al ratio during synthesis and adjusting its physicochemical characteristics.<sup>54</sup> However, the Ni–Al LDH demonstrated limited solar light utilization, which primarily absorbs the light in the UV spectrum.<sup>55</sup> Thus, it is of great importance to choose suitable semiconductors with an extended light absorption range to construct Ni–Al LDH-based heterojunctions.

## 4. Conclusions and perspectives

This work sheds light on current advances in Ni–Al LDH-based heterojunctions for boosting solar energy consumption, facilitating charge migration, strengthening photostability, enhancing photocatalytic performance, and addressing the energy crisis and environmental issue. Thus, Ni–Al LDH-based heterojunctions have been widely employed for photocatalytic CO<sub>2</sub> reduction, H<sub>2</sub> evolution, and pollution degradation due to their large surface area, tunable bandgap and morphology, abundant reaction sites, and high activity, selectivity, and photostability. Although significant progress has been demonstrated in the construction and research of Ni–Al LDH-based heterojunctions in recent years, they still need to be further investigated and a substantial amount of challenges and bottlenecks still need to be overcome: (i) limitations in light absorption further complicate matters; (ii) there is little theoretical information about Ni–Al LDH-based heterojunctions; (iii) the photocatalytic mechanism especially the charge transfer route is unclear; (iv) most Ni–Al LDH-based heterojunctions with nanosheet-like and microsphere structures exhibit low surface area; (v) electron transfer and migration in the Ni–Al LDH-based heterojunction occurs through multiple intermediates, leading to energy loss.

## Data availability

No primary research results, software or code have been included and no new data were generated or analysed as part of this review.

## Conflicts of interest

The authors declare no conflicts of interest.

## Acknowledgements

This work was supported by the Natural Science Foundation of Fujian Province (grant no. 2023J05052) and the School of Chemistry and Chemical Engineering/State Key Laboratory Incubation Base for Green Processing of Chemical Engineering, Shihezi, 832003, China.

## References

- J. Zhang, Y. Yang, G. Ding, Z. Wang, P. Wang, C. Li and G. Liao, *Chem. Eng. J.*, 2025, DOI: [10.1016/j.cej.2024.159165](https://doi.org/10.1016/j.cej.2024.159165).
- G. Ding, Z. Wang, J. Zhang, P. Wang, L. Chen and G. Liao, *EcoEnergy*, 2024, **2**, 22–44.
- B. H. Graimed, Z. H. Jabbar, A. A. G. Al-Khayfawee, S. H. Ammar, H. Taofeeq and M. Al-Yasiri, *Int. J. Hydrogen Energy*, 2024, **87**, 939–965.
- S. Iguchi, S. Kikkawa, K. Teramura, S. Hosokawa and T. Tanaka, *Phys. Chem. Chem. Phys.*, 2016, **18**, 13811–13819.
- S.-M. Xu, T. Pan, Y.-B. Dou, H. Yan, S.-T. Zhang, F.-Y. Ning, W.-Y. Shi and M. Wei, *J. Phys. Chem. C*, 2015, **119**, 18823–18834.
- Y. R. Dias and O. W. Perez-Lopez, *J. CO<sub>2</sub> Util.*, 2023, **68**, 102381.
- U. A. Mohanty, D. P. Sahoo, L. Paramanik and K. Parida, *Sustainable Energy Fuels*, 2023, **7**, 1145–1186.
- Y. Wu, P. Zhu, Y. Li, L. Zhang and Z. Jin, *ACS Appl. Energy Mater.*, 2022, **5**, 8157–8168.
- X. Deng, C. Liu, X. Yan, J. Fan, Q. Liang and Z. Li, *Chin. Chem. Lett.*, 2024, **35**, 108942.
- X. Li, J. Yu and M. Jaroniec, *Chem. Soc. Rev.*, 2016, **45**, 2603–2636.
- G. Liao, G. Ding, B. Yang and C. Li, *Precis. Chem.*, 2024, **2**, 49–56.
- G. Liao, Y. He, H. Wang, B. Fang, N. Tsubaki and C. Li, *Device*, 2023, **1**, 100173.
- G. Ding, C. Li, L. Chen and G. Liao, *Energy Environ. Sci.*, 2024, **17**, 5311–5335.
- C. Li, G. Ding, X. Liu, P. Huo, Y. Yan, Y. Yan and G. Liao, *Chem. Eng. J.*, 2022, **435**, 134740.
- H. Zhu, C. Zhang, K. Xie, X. Li and G. Liao, *Chem. Eng. J.*, 2023, **453**, 139775.
- C. Dette, M. A. Pérez-Osorio, C. S. Kley, P. Punke, C. E. Patrick, P. Jacobson, F. Giustino, S. J. Jung and K. Kern, *Nano Lett.*, 2014, **14**, 6533–6538.
- H. Zhang, Z. Wang, J. Zhang and K. Dai, *Chin. J. Catal.*, 2023, **49**, 42–67.
- G. Liao, C. Li, S.-Y. Liu, B. Fang and H. Yang, *Phys. Rep.*, 2022, **983**, 1–41.
- C. Li, H. Lu, G. Ding, T. Ma, S. Liu, L. Zhang and G. Liao, *Chin. J. Catal.*, 2024, **65**, 174–184.
- K. Xu, Z. Zhu, C. Hu, J. Zheng, H. Peng and B. Liu, *Colloids Surf., A*, 2023, **674**, 131806.
- B. Ma, C. Zhang, D. Jia, Q. Zhao and P. Yang, *J. Phys. Chem. C*, 2023, **127**, 2908–2917.
- M. Yang, X. Zhu, Z. Zhu, H. Zhang, Y. Teng, D.-B. Kuang and Y. Li, *Chem. Eng. J.*, 2023, **472**, 145071.
- W. Zhang, Y. Meng, Y. Liu, H. Shen, Z. Ni, S. Xia, W. Han, Y. Li and H. Tang, *J. Environ. Chem. Eng.*, 2022, **10**, 107812.
- Y. Fu, Y. Li, J. Zhang, D. Liu, C. Liu and Y. Ke, *Inorg. Chem. Commun.*, 2022, **142**, 109651.
- G. Liao, Y. Gong, L. Zhang, H. Gao, G.-J. Yang and B. Fang, *Energy Environ. Sci.*, 2019, **12**, 2080–2147.
- C. Li, H. Lu, G. Ding, Q. Li and G. Liao, *Catal. Sci. Technol.*, 2023, **13**, 2877–2898.
- C. Sun, L. Wu, J. Hu, S. A. Hussain, J. Yang and F. Jiao, *Chem. Eng. J.*, 2023, **474**, 145616.
- X. Cao, Y. Qiao, M. Jia, P. He and H. Zhou, *Adv. Energy Mater.*, 2022, **12**, 2003972.
- G. Ding, C. Li, Y. Ni, L. Chen, L. Shuai and G. Liao, *EES Catal.*, 2023, **1**, 369–391.
- R. Dang, X.-R. Ma, Y.-P. Zhao, M. Ren, W. Guo, Y.-H. Kang, Y. Gao, S. Bi, W. Gao, H.-R. Hao, R. Bai, Y.-F. Wang, L. Yan,

- L. Gao, Z.-F. Zhang, Y.-J. Ma and X.-Y. Wei, *Chem. Eng. J.*, 2023, **451**, 138499.
- 31 C. Li, R. Jia, Y. Yang and G. Liao, *Adv. Fiber Mater.*, 2023, **5**, 1549–1551.
- 32 Z. Yan, B. Song, G. Fang, T. Wu, N. Chen, M. Zhao, X. Zou and G. Liao, *ACS Sustainable Chem. Eng.*, 2021, **9**, 10403–10423.
- 33 Q. Ma, X. Han, J. Cui, Y. Zhang and W. He, *Colloids Surf., A*, 2022, **649**, 129270.
- 34 H. Zhu, L. Gou, C. Li, X. Fu, Y. Weng, L. Chen, B. Fang, L. Shuai and G. Liao, *Device*, 2024, **2**, 100283.
- 35 G. Liao and M. Wu, *Innovation Energy*, 2024, **1**, 100047.
- 36 C. Li, B. Cheng, H. Lu, G. Ding, Z. Jiang and G. Liao, *Inorg. Chem.*, 2023, **62**, 6843–6850.
- 37 Y. Liu, X. Ma and Z. Jin, *J. Colloid Interface Sci.*, 2022, **609**, 686–697.
- 38 G. Liao, C. Li, X. Li and B. Fang, *Cell Rep. Phys. Sci.*, 2021, **2**, 100355.
- 39 G. Liao, C. Li, S.-Y. Liu, B. Fang and H. Yang, *Trends Chem.*, 2022, **4**, 111–127.
- 40 S. Megala, P. Ravi, P. Maadeswaran, M. Navaneethan, M. Sathish and R. Ramesh, *Nanoscale Adv.*, 2021, **3**, 2075–2088.
- 41 F. Tian, X. Wu, J. Chen, X. Sun, X. Yan and G. Liao, *Dalton Trans.*, 2023, **52**, 11934–11940.
- 42 Q. Zhang, G. Liao, B. Yang, Y. Zhang, G. Ge, A. Lipovka, J. Liu, R. D. Rodriguez, X. Yang and X. Jia, *Appl. Surf. Sci.*, 2023, **638**, 157989.
- 43 S. Zhao, D. Pan, Q. Liang, M. Zhou, C. Yao, S. Xu and Z. Li, *J. Phys. Chem. C*, 2021, **125**, 10207–10218.
- 44 X.-y. Ji, R.-t. Guo, J.-y. Tang, Y.-f. Miao, Z.-d. Lin, L.-f. Hong, Y. Yuan, Z.-s. Li and W.-g. Pan, *ACS Appl. Energy Mater.*, 2022, **5**, 2862–2872.
- 45 X. Chen, B. Fan, H. Wang, X. Liu, Y. Liu and J. Gao, *Inorg. Chem.*, 2024, **63**, 5132–5141.
- 46 K. Liu, Y. Liao, P. Wang, X. Fang, J. Zhu, G. Liao and X. Xu, *Nanoscale*, 2024, **16**, 11096–11108.
- 47 C. Li, N.-Y. Huang, Y. Yang, Q. Xu and G. Liao, *Coord. Chem. Rev.*, 2025, **524**, 216292.
- 48 W.-K. Jo, S. Moru and S. Tonda, *J. Mater. Chem. A*, 2020, **8**, 8020–8032.
- 49 S. Liu, Y. Guo, S. Yi, S. Yan, C. Ouyang, F. Deng, C. Li, G. Liao and Q. Li, *Sep. Purif. Technol.*, 2023, **307**, 122727.
- 50 G. Salehi, R. Abazari and A. R. Mahjoub, *Inorg. Chem.*, 2018, **57**, 8681–8691.
- 51 C. Sun, J. Hu, L. Wu, Q. Xia and F. Jiao, *Ind. Eng. Chem. Res.*, 2023, **62**, 466–477.
- 52 K. S. Novoselov, A. Mishchenko, A. Carvalho and A. H. C. Neto, *Science*, 2016, **353**, aac9439.
- 53 W. Wang and J. Yao, *Appl. Clay Sci.*, 2024, **260**, 107519.
- 54 L. Yang, L. Li, P. Xia, H. Li, J. Yang, X. Li, X. Zeng, X. Zhang, C. Xiao and Y. Xie, *Chem. Commun.*, 2021, **57**, 11629–11632.
- 55 F. Beigi, A. R. Mahjoub and A. H. C. Khavar, *Appl. Surf. Sci.*, 2023, **637**, 157972.